materials

MDPI

Article

Investigation of Superconductivity in Ce-Doped (La,Pr)$OBiS_2$ Single Crystals

Masanori Nagao [1,2,*], Yuji Hanada [1], Akira Miura [3], Yuki Maruyama [1], Satoshi Watauchi [1], Yoshihiko Takano [2] and Isao Tanaka [1]

[1] Center for Crystal Science and Technology, University of Yamanashi, 7-32 Miyamae, Kofu 400-0021, Japan; g20dte03@yamanashi.ac.jp (Y.H.); myuuki@yamanashi.ac.jp (Y.M.); watauchi@yamanashi.ac.jp (S.W.); itanaka@yamanashi.ac.jp (I.T.)
[2] International Center for Materials Nanoarchitectonics (MANA), National Institute for Materials Science, 1-2-1 Sengen, Tsukuba 305-0047, Japan; takano.yoshihiko@nims.go.jp
[3] Faculty of Engineering, Hokkaido University, Kita-13 Nishi-8, Kita-ku, Sapporo 060-8628, Japan; amiura@eng.hokudai.ac.jp
* Correspondence: mnagao@yamanashi.ac.jp; Tel.: +81-55-220-8610; Fax: +81-55-220-8270

Abstract: Single crystals of Ce-doped (La,Pr)$OBiS_2$ superconductors, the multinary rare-earth elements substituted *R*$OBiS_2$, were successfully grown. The grown crystals typically had a size of 1–2 mm and a plate-like shape with a well-developed *c*-plane. The c-axis lattice constants of the obtained (La,Ce,Pr)$OBiS_2$ single crystals were approximately 13.6–13.7 Å, and the superconducting transition temperature was 1.23–2.18 K. Valence fluctuations of Ce and Pr were detected through X-ray absorption spectroscopy analysis. In contrast to (Ce,Pr)$OBiS_2$ and (La,Ce)$OBiS_2$, the superconducting transition temperature of (La,Ce,Pr)$OBiS_2$ increased with the increasing concentrations of the tetravalent state at the *R*-site.

Keywords: superconducting-related materials; single crystal growth; valence fluctuation

Citation: Nagao, M.; Hanada, Y.; Miura, A.; Maruyama, Y.; Watauchi, S.; Takano, Y.; Tanaka, I. Investigation of Superconductivity in Ce-Doped (La,Pr)$OBiS_2$ Single Crystals. *Materials* **2022**, *15*, 2977. https://doi.org/10.3390/ma15092977

Academic Editor: Dominique de Caro

Received: 22 March 2022
Accepted: 18 April 2022
Published: 19 April 2022

1. Introduction

Layered superconductors, such as cuprate [1–3] and iron-based superconductors [4,5], often exhibit high superconducting transition temperatures. Research on layered superconductors is important in order to understand materials that have high superconducting transition temperatures. *R*(O,F)BiS_2 (*R*: rare-earth elements) compounds are layered superconductors and BiS_2-based superconductors, and their superconductivity is triggered by substituting F at the O site [6–11]. A similar superconducting analogy is found in iron-based superconductors [5]. On the other hand, one of the BiS_2-based superconductors, $CeOBiS_2$, exhibits superconductivity without F substitution owing to the valence fluctuation between Ce^{3+} and Ce^{4+} [12,13]. Thus, F-free *R*$OBiS_2$ compounds with partial Ce substitution at the *R*-site also become superconductors in the form of the (La,Ce)$OBiS_2$ [14], (Ce,Pr)$OBiS_2$ [15,16], (Ce,Nd)$OBiS_2$ [17], and (La,Ce,Pr,Nd,Sm)$OBiS_2$ [18] compounds. Moreover, *R*-site elements affect the superconducting transition temperature. Knowledge of the superconductivity of F-free *R*$OBiS_2$ compounds is important for understanding BiS_2-based superconductors. F-free *R*$OBiS_2$ compounds with *R* = La, Ce, Pr have been obtained [12,13,19,20], but those of *R* = Nd, Sm have never been synthesized. Therefore, we focused on (La,Ce,Pr)$OBiS_2$ single crystals.

In this paper, we successfully grew F-free (La,Ce,Pr)$OBiS_2$ and (La,Pr)$OBiS_2$ single crystals using a CsCl and a KCl flux, respectively. Hereafter, we denote binary and ternary *R*$OBiS_2$ by the number of *R* elements: binary—(La,Ce)$ObiS_2$, (Ce,Pr)$ObiS_2$, and (La,Pr)$OBiS_2$; ternary—(La,Ce,Pr)$OBiS_2$. The obtained ternary single crystals of (La,Ce,Pr)$OBiS_2$ were characterized by X-ray absorption fine structure (XAFS) spectroscopy for the Ce and Pr valence and the electrical transport properties down to approximately

0.2 K. The properties of the ternary (La,Ce,Pr)$OBiS_2$ were investigated in comparison with those of binary *R*$OBiS_2$ systems—namely, (La,Ce)$OBiS_2$, (Ce,Pr)$OBiS_2$, and (La,Pr)$OBiS_2$. The relationship between the *R*-site valence state and the superconducting transition temperature (T_c) for (La,Ce,Pr)$OBiS_2$ was observed using the single crystals obtained.

2. Experimental

(La,Ce,Pr)$OBiS_2$ and (La,Pr)$OBiS_2$ single crystals were grown through a high-temperature flux method [12,20–22]. The raw materials—La_2S_3 (99.9 wt%), Ce_2S_3 (99.9 wt%), Pr_2S_3 (99.9 wt%), Bi_2O_3 (99.9 wt%), and Bi_2S_3 (99.9 wt%)—were weighed for a nominal composition of $La_aCe_bPr_cOBiS_2$ ($a + b + c = 1.0$). The mixture of the raw materials (0.8 g) and alkali metal chloride flux (5.0 g) was ground using a mortar and then sealed into an evacuated quartz tube (~10 Pa). The alkali metal chloride fluxes for the single crystal growths of (La,Ce,Pr)$OBiS_2$ and (La,Pr)$OBiS_2$ were CsCl (99.8 wt%) and KCl (99.5 wt%), respectively. The quartz tube was heated at T_{max} °C for 10 h, followed by a cooling to T_{end} °C at a rate of 1 °C/h. The T_{max} values for (La,Ce,Pr)$OBiS_2$ and (La,Pr)$OBiS_2$ were 950 °C and 1050 °C, respectively. The value of T_{end} depends on the melting temperature of the flux. In consequence, we adopted 650 °C and 750 °C for (La,Ce,Pr)$OBiS_2$ and (La,Pr)$OBiS_2$, respectively. The samples were then furnace-cooled to room temperature. The resulting quartz tube was opened in an air atmosphere, and the obtained products were washed and filtered by distilled water to remove the alkali metal chloride flux.

The compositional ratio of the single crystals was evaluated by energy-dispersive X-ray spectrometry (EDS) (Bruker; Quantax 70) associated with the observation of the microstructure using a scanning electron microscope (SEM) (Hitachi High-Technologies; TM3030). The obtained compositional values were normalized using La + Ce + Pr = 1.00, with the Bi and S values measured to a precision of two decimal places. The identification and evaluation of the orientation of the grown crystals were performed with X-ray diffraction (XRD) using Rigaku MultiFlex with Cu Kα radiation. The superconducting transition temperature (T_c) with zero resistivity was determined by the resistivity–temperature (ρ–T) characteristics. The ρ–T characteristics were measured using the standard four-probe method with a constant current density (J) mode and a physical property measurement system (Quantum Design; PPMS DynaCool). The electrical terminals were fabricated with Ag paste. The ρ–T characteristics in the temperature range 0.2–15 K were measured with an adiabatic demagnetization refrigerator (ADR) option for PPMS. The magnetic field for the operation of the ADR, 3 T at 1.9 K, was applied and subsequently removed. The temperature of the sample consequently decreased to approximately 0.2 K. The measurement of the ρ–T characteristics was begun at the lowest temperature (~0.2 K), which was spontaneously increased to 15 K. The valence state of the rare-earth elements (Ce, Pr) in the grown crystals was estimated using the X-ray absorption fine structure (XAFS) spectroscopy analysis with an Aichi XAS beamline and synchrotron X-ray radiation (BL5S1 and BL11S2). For the XAFS spectroscopy sample, the obtained single crystals were ground, mixed with boron nitride (BN) powder, and pressed into a pellet with a diameter of 4 or 10 mm.

3. Results and Discussion

Figure 1 shows a typical SEM image of the (La,Ce,Pr)$OBiS_2$ single crystal. The obtained single crystals had plate-like shapes with sizes and thicknesses in the ranges of 1–2 mm and 100–400 μm, respectively. On the other hand, the obtained (La,Pr)$OBiS_2$ single crystals exhibited plate-like shapes and were thin compared to the (La,Ce,Pr)$OBiS_2$ single crystals. (La,Pr)$OBiS_2$ single crystals became thick with increasing La contents. The ranges of their size and thickness were 0.5–1.0 mm and 10–200 μm, respectively.

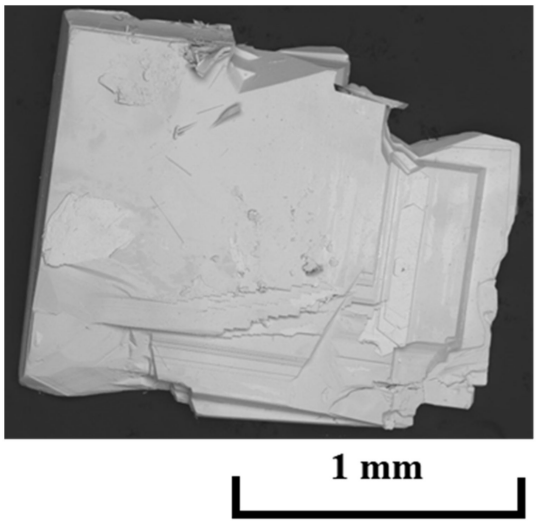

Figure 1. Typical SEM image of a (La,Ce,Pr)$OBiS_2$ single crystal.

Figure 2 shows the typical XRD patterns of a well-developed plane in the (La,Ce,Pr)$OBiS_2$ and (La,Pr)$OBiS_2$ single crystals obtained. The presence of only the 00*l* diffraction peaks, similar to $CeOBiS_2$ compound structures [12], indicated a well-developed *c*-plane. The *c*-axis lattice constants of (La,Ce,Pr)$OBiS_2$ and (La,Pr)$OBiS_2$ single crystals were in the ranges of 13.59–13.68 Å and 13.80–13.81 Å, respectively. The differences between the *c*-axis lattice constants in the grown (La,Pr)$OBiS_2$ single crystals were small, even though the compositions of the crystals varied extensively. Those values and the defined sample names are shown in Table 1. The analyzed atomic ratios of rare-earth elements in the grown (La,Ce,Pr)$OBiS_2$ and (La,Pr)$OBiS_2$ single crystals did not correspond precisely to the nominal compositions. The nominal compositions and the analyzed averaging compositions of the rare-earth elements are shown in Table 1. The estimated atomic ratios of the Bi and S elements in the obtained single crystals were Bi:S = 1.01 ± 0.05:2.01 ± 0.04, which agrees with the nearly stoichiometric ratio. On the other hand, Cs, K, and Cl from the flux were not detected in the single crystals with a minimum sensitivity limit of approximately 1 wt%.

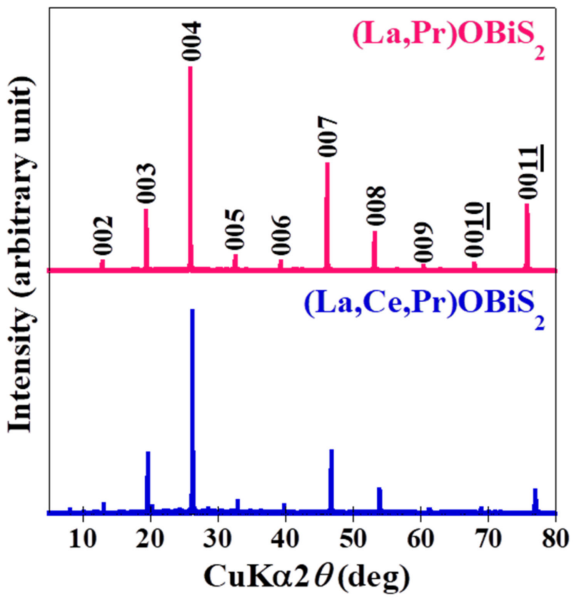

Figure 2. Typical XRD pattern of a well-developed plane of (La,CePr)$OBiS_2$ and (La,Pr)$OBiS_2$ single crystals.

Table 1. Nominal compositions and analyzed compositions at the *R*-site, and *c*-axis lattice constants in the grown single crystals.

Sample Name	Nominal Compositions			Analyzed Compositions			*c*-Axis Lattice Constants (Å)
	La:*a*	Ce:*b*	Pr:*c*	La	Ce	Pr	
#1	0.10	0.20	0.70	0.13 ± 0.01	0.20 ± 0.01	0.67 ± 0.02	13.68
#2	0.25	0.50	0.25	0.20 ± 0.02	0.60 ± 0.03	0.20 ± 0.02	13.59
#3	0.33	0.33	0.33	0.31 ± 0.01	0.35 ± 0.04	0.34 ± 0.05	13.61
#4	0.65	0.15	0.20	0.69 ± 0.03	0.13 ± 0.01	0.18 ± 0.04	13.68
#5	0.10	0	0.90	0.28 ± 0.02	0	0.72 ± 0.03	13.80
#6	0.50	0	0.50	0.60 ± 0.02	0	0.40 ± 0.01	13.80
#7	0.90	0	0.10	0.89 ± 0.03	0	0.11 ± 0.03	13.81

Figure 3 shows the ρ–T characteristics parallel to the *c*-plane in the temperature range 0.2–15 K for the $La_{0.31}Ce_{0.35}Pr_{0.34}OBiS_2$ and $La_{0.60}Pr_{0.40}OBiS_2$ single crystals, which were typical (La,Ce,Pr)$OBiS_2$ and (La,Pr)$OBiS_2$ single crystals, respectively. $La_{0.31}Ce_{0.35}Pr_{0.34}OBiS_2$ single crystals exhibited superconductivity, but no superconducting transition was observed down to 0.2 K in $La_{0.60}Pr_{0.40}OBiS_2$ single crystals. The electrical resistivity slightly increased with the decreasing temperature, indicating a semiconducting behavior in the normal state. The resistivity of (La,Ce,Pr)$OBiS_2$ single crystals in a normal state was far lower than that of (La,Pr)$OBiS_2$. For this reason, we assumed that the carrier was induced because of the Ce valence fluctuation. The Ce valence state will be exhibited in Figure 5. The other obtained (La,Ce,Pr)$OBiS_2$ and (La,Pr)$OBiS_2$ single crystals also demonstrated similar behavior, except for the T_c. Figure 4 shows the relationship between the superconducting transition temperature (T_c) and the compositions of the rare-earth elements (La, Ce, Pr) analyzed for the binary and ternary *R*$OBiS_2$ single crystals plotted on the ternary diagrams. The T_c values of (La,Ce)$OBiS_2$ and (Ce,Pr)$OBiS_2$ from previous reports are also shown in Figure 4 [12–16,19,20]. Superconductivity was not observed down to 0.2 K for the grown Ce-free *R*$OBiS_2$ single crystals, which were (La,Pr)$OBiS_2$ single crystals. On the other hand, the obtained (La,Ce,Pr)$OBiS_2$ single crystals exhibited T_c values of 1.23–2.18 K. In the rare-earth element composition, T_c disappeared near the region with higher La contents. On the other hand, T_c was increased by increasing the Pr content. When the composition of the *R*-site became $Ce_{0.1}Pr_{0.9}$, T_c exhibited its maximum value. However, no superconductivity was observed in the end-component $PrOBiS_2$ [20]. Furthermore, these results indicate that Ce substitution is required for superconductivity in binary and ternary *R*$OBiS_2$. The $CeOBiS_2$ superconductor was induced into superconductivity by a Ce valence fluctuation caused by a mixture state of trivalent (Ce^{3+}) and tetravalent (Ce^{4+}) electronic configurations [13]. Thus, we focused on the valence state of rare-earth elements in (La,Ce,Pr)$OBiS_2$ single crystals.

Figure 5 shows (a) the Ce L_3-edge and (b) the Pr L_3-edge absorption spectra of the grown (La,Ce,Pr)$OBiS_2$ single crystals and standard samples for each valence state using XAFS spectroscopy analysis at room temperature. The Ce L_3-edge of the grown (La,Ce,Pr)$OBiS_2$ single crystals demonstrated a peak at around 5725 eV and was assigned to trivalent electronic configuration (Ce^{3+}) [23]. Moreover, the peaks around 5730 eV and 5737 eV were assigned to tetravalent electronic configuration (Ce^{4+}) [24]. All grown (La,Ce,Pr)$OBiS_2$ single crystals exhibited a Ce valence fluctuation caused by a mixture state of Ce^{3+} and Ce^{4+}. The Ce valence states in the grown (La,Ce,Pr)$OBiS_2$ single crystals were analyzed using linear combination fitting of Ce_2S_3 (Ce^{3+}) and CeO_2 (Ce^{4+}) through XAFS spectroscopy spectra. In the tetravalent electronic configuration (Ce^{4+}) peak, samples #2 and #3 demonstrated values around 5737 eV, which were low compared to those of other samples. The values of the Ce^{4+} concentrations at the *R*-site for these samples were close to those for samples #1 and #4, but the Ce element concentrations at the *R*-site were higher than those for samples #1 and #4 (See Table 2). In consequence, the Ce^{4+}/Ce^{3+} ratios of samples #2 and #3 were smaller than those of samples #1 and #4. Therefore, the Ce^{4+} peaks became lower relative to those of samples #1 and #4. On the other hand, the Pr L_3-edge

of those single crystals exhibited a peak at approximately 5966 eV, which was assigned to the trivalent electronic configuration (Pr^{3+}) [25,26]. Moreover, the tetravalent electronic configuration (Pr^{4+}) demonstrated a peak at approximately 5978 eV in Pr_6O_{11} [25,27]. The Pr valence states were also analyzed using a linear combination fitting of Pr_2S_3 (Pr^{3+}) and Pr_6O_{11} (one-third Pr^{3+} and two-thirds Pr^{4+}). In consequence, the trivalent electronic structure was dominant, but a low concentration of the tetravalent electronic configuration was found. In a similar fashion, the Pr valence states in the grown (La,Pr)$OBiS_2$ single crystals were analyzed. The tetravalent electronic structure (Pr^{4+}) concentrations were low, as shown in Figure 6. The tetravalent electronic configuration (R^{4+}) concentrations and the mean *R*-site ionic radius considering the valence state (R^{3+} and R^{4+}) for the grown single crystals are summarized in Table 2. Exceptionally, the concentrations of Pr^{4+} in sample #1 ($R = La_{0.13}Ce_{0.20}Pr_{0.67}$) and sample #5 ($R = La_{0.28}Pr_{0.72}$) were high, with both at approximately 10% at the *R*-site. The T_c of sample #1 exhibited comparatively high, but sample #5 did not exhibit superconductivity. Even though this observation still requires clarification, it provides important information on the superconducting mechanism of BiS_2-based materials.

Herein, we discuss the effect of valence states and ionic radius on binary and ternary *R*$OBiS_2$. Figure 7 shows the dependence of the tetravalent electronic configuration (R^{4+}) concentrations on T_c for the binary and ternary *R*$OBiS_2$ single crystals. While binary *R*$OBiS_2$ exhibits little correlation between the ratio of tetravalent ions and T_c, ternary *R*$OBiS_2$ demonstrates a clear correlation between them; an increased ratio of tetravalent ions increased T_c. This result indicates that the electronic state of ternary *R*$OBiS_2$ is different from that of binary *R*$OBiS_2$. Figure 8 shows the relationship between the mean *R*-site ionic radius [28] considering the valence state (R^{3+} and R^{4+}) and the T_c for binary and ternary *R*$OBiS_2$ single crystals. The T_c decreased with an increase in the mean *R*-site ionic radius. Although some anomalous data have been noted, this trend was consistent with the chemical pressure effect at the *R*-site [29]. There was no significant difference in terms of ionic radius between binary and ternary *R*$OBiS_2$. Thus, ternary *R*$OBiS_2$ is more sensitive to the electronic configuration, while both binary and ternary *R*$OBiS_2$ have similar trends in their ionic radius. Additionally, these results reveal that Ce-substitution at the *R*-site is required for superconductivity.

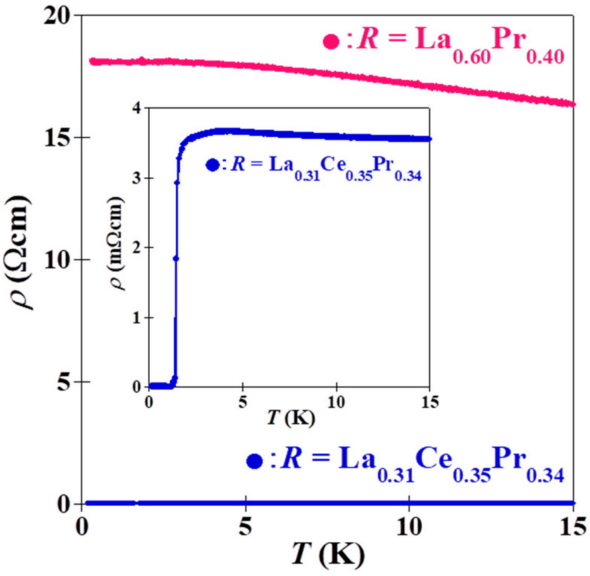

Figure 3. ρ–T characteristics parallel to the *c*-plane in the temperature range 0.2–15 K for the $La_{0.31}Ce_{0.35}Pr_{0.34}OBiS_2$ and $La_{0.60}Pr_{0.40}OBiS_2$ single crystals. The inset is an enlargement of the lower-resistivity region.

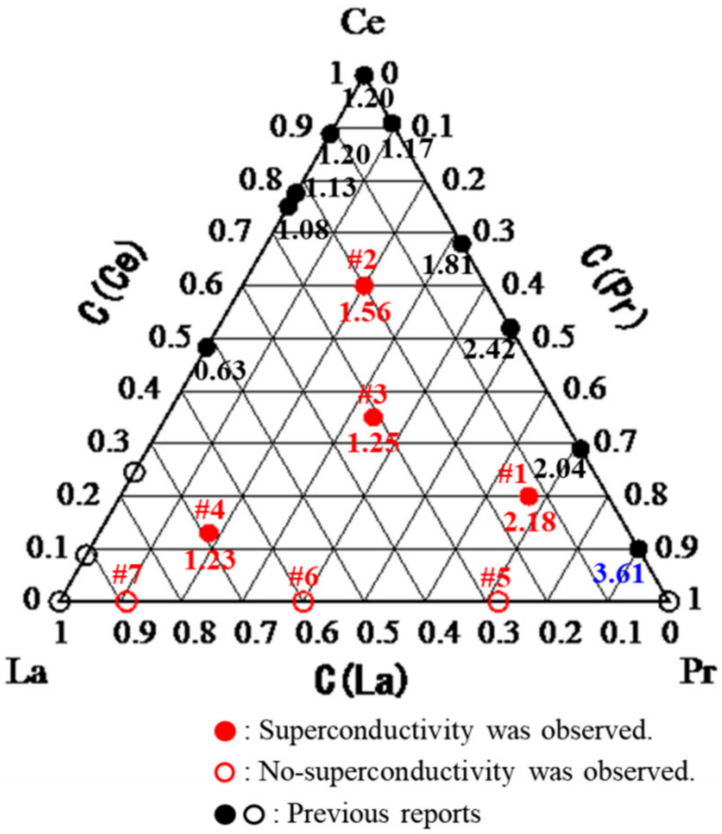

Figure 4. Relationship between the superconducting transition temperature (T_c) and the compositions of the rare-earth elements (La,Ce,Pr) analyzed. The values in the ternary diagram are T_c^{zero}, in kelvin (K).

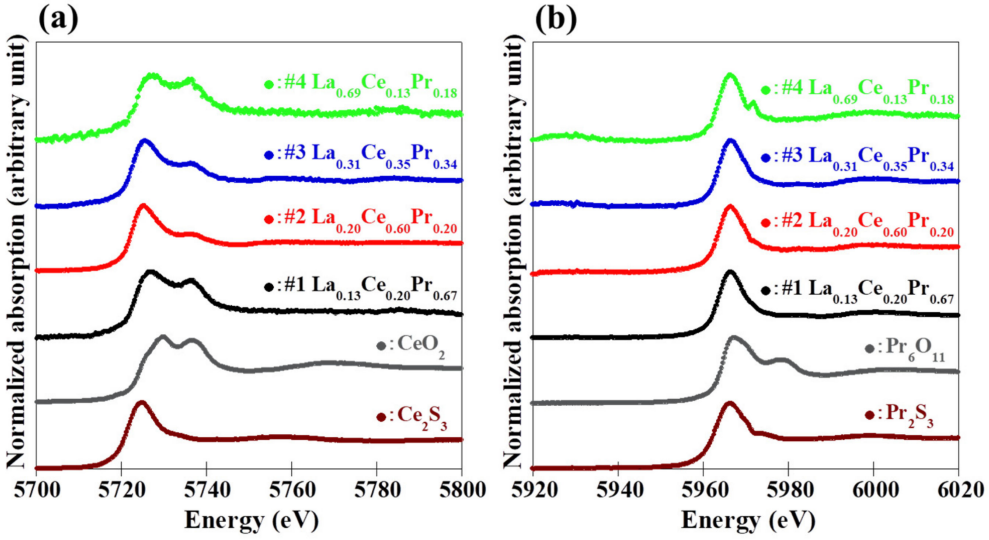

Figure 5. (**a**) Ce L_3-edge and (**b**) Pr L_3-edge absorption spectra using XAFS spectroscopy at room temperature for the grown (La,Ce,Pr)$OBiS_2$ single crystals and standard samples for each valence state (Ce^{3+}: Ce_2S_3; Ce^{4+}: CeO_2; and Pr^{3+}: Pr_2S_3; Pr^{4+}: Pr_6O_{11}).

Table 2. Tetravalent electronic configuration (R^{4+}) concentrations at the *R*-site, and mean *R*-site ionic radius considering the valence state (R^{3+} and R^{4+}) for the grown single crystals.

Sample Name	Analyzed Averaging Compositions			Tetravalent Electronic Configuration (R^{4+}) Concentrations at the *R*-Site			Mean *R*-Site Ionic Radius (Å)
	La	Ce	Pr	Ce^{4+}	Pr^{4+}	Total (Ce^{4+}+Pr^{4+})	
#1	0.13	0.20	0.67	0.13	0.11	0.24	0.966
#2	0.20	0.60	0.20	0.16	0.01	0.17	0.987
#3	0.31	0.35	0.34	0.11	0.03	0.14	0.991
#4	0.69	0.13	0.18	0.09	0.01	0.10	1.01
#5	0.28	0	0.72	0	0.09	0.09	0.989
#6	0.60	0	0.40	0	0	0	1.02
#7	0.89	0	0.11	0	0.01	0.01	1.03

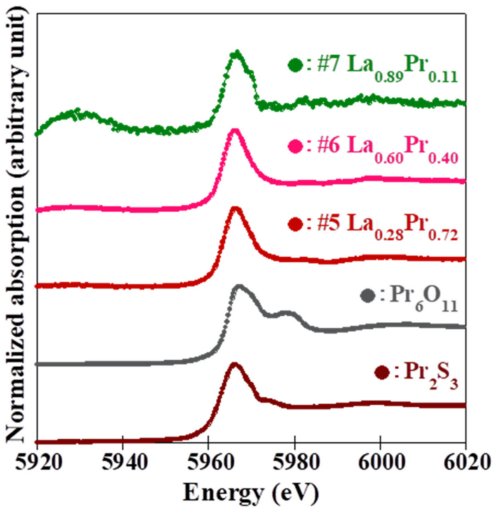

Figure 6. Pr L_3-edge absorption spectra using XAFS spectroscopy at room temperature for the grown (La,Pr)$OBiS_2$ single crystals, Pr_2S_3 and Pr_6O_{11}.

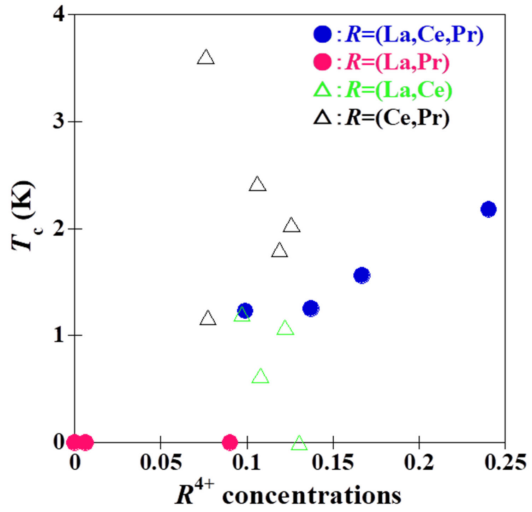

Figure 7. Dependence of the tetravalent electronic configuration (R^{4+}) concentrations on T_c for the binary and ternary $ROBiS_2$ single crystals.

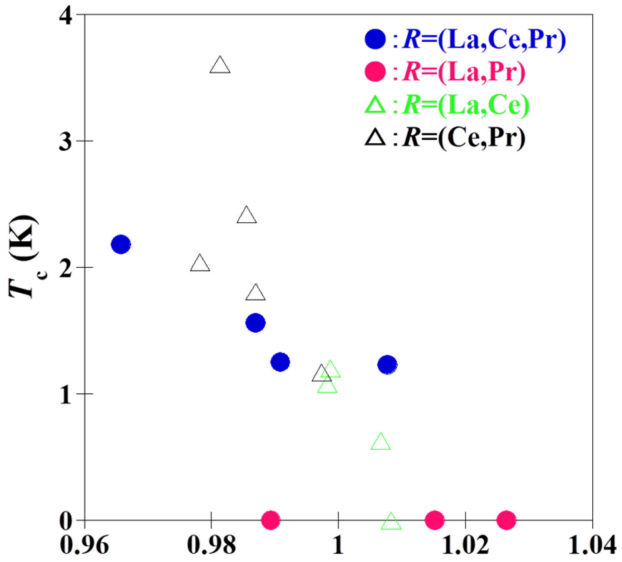

Figure 8. Relationship between the mean *R*-site ionic radius considering the valence state (R^{3+} and R^{4+}) and the T_c for the binary and ternary ROBiS$_2$ single crystals.

4. Conclusions

(La,Ce,Pr)OBiS$_2$ and (La,Pr)OBiS$_2$ single crystals were successfully grown using a CsCl and a KCl flux, respectively. The superconducting transition temperature of the grown (La,Ce,Pr)OBiS$_2$ single crystals was 1.23–2.18 K. (La,Pr)OBiS$_2$ single crystals exhibited no superconductivity down to 0.2 K. The requirement of Ce substitution was revealed for the induction of superconductivity in binary and ternary ROBiS$_2$. In the (La,Ce,Pr)OBiS$_2$ and (La,Pr)OBiS$_2$ single crystals, the Ce valence fluctuation was much larger than that of Pr, except for particular samples. For the ternary ROBiS$_2$ (R = La + Ce + Pr) single crystals, the superconducting transition temperature increased with increasing concentrations of the tetravalent state (R^{4+}) at the *R*-site, but the binary ROBiS$_2$ (R = La + Ce, Ce + Pr, La + Pr) demonstrated no such correlation. According to the investigation of the mean *R*-site ionic radius, these superconducting transition temperature behaviors were found to be similar to the trend of the chemical pressure effect at the *R*-site. The superconducting transition temperature of ROBiS$_2$ (R = La, Ce, Pr) did not demonstrate a simple dependence on the carrier concentration of the tetravalent state (R^{4+}) at the *R*-site, but it may be easy to tune by varying the mean *R*-site ionic radius.

Author Contributions: Conceptualization, M.N.; Methodology, M.N.; Validation, M.N. and Y.H.; Formal analysis, M.N., Y.H. and A.M.; Investigation, M.N. and A.M.; Resources, Y.M., S.W., Y.T. and I.T.; Data curation, M.N. and Y.H.; Writing—original draft preparation, M.N.; Writing—review and editing, A.M., S.W., I.T.; Visualization, M.N.; Supervision, Y.M., S.W., Y.T. and I.T.; Project administration, M.N.; Funding acquisition, M.N., A.M. and I.T. All authors have read and agreed to the published version of the manuscript.

Funding: This work was partially supported by JSPS KAKENHI (Grant-in-Aid for Scientific Research (B) and (C)), Grant Number 21H02022 and 19K05248.

Institutional Review Board Statement: Not applicable.

Informed Consent Statement: Not applicable.

Acknowledgments: The XAFS spectroscopy experiments were conducted at the BL11S2 and BL5S1 of the Aichi Synchrotron Radiation Center, Aichi Science & Technology Foundation, Aichi, Japan (Experimental No. 201801025 and No. 202005002).

Conflicts of Interest: The authors declare no conflict of interest.

References

1. Bednorz, J.G.; Müller, K.A. Possible highT_c superconductivity in the Ba−La−Cu−O system. *Phys. B Condens. Matter* **1986**, *64*, 189–193. [CrossRef]
2. Wu, M.K.; Ashburn, J.R.; Thorng, C.J.; Hor, P.H.; Meng, R.L.; Gao, L.; Huang, Z.J.; Wang, Y.Q.; Chu, C.W. Superconductivity at 93 K in a new mixed-phase Y-Ba-Cu-O compound system at ambient pressure. *Phys. Rev. Lett.* **1987**, *58*, 908. [CrossRef] [PubMed]
3. Maeda, H.; Tanaka, Y.; Fukutomi, M.; Asano, T. A New High-T_c Oxide Superconductor without a Rare Earth Element. *Jpn. J. Appl. Phys.* **1988**, *27*, L209. [CrossRef]
4. Kamihara, Y.; Hiramatsu, H.; Hirano, M.; Kawamura, R.; Yanagi, H.; Kamiya, T.; Hosono, H. Iron-Based Layered Superconductor: LaOFeP. *J. Am. Chem. Soc.* **2006**, *128*, 10012–10013. [CrossRef]
5. Kamihara, Y.; Watanabe, T.; Hirano, M.; Hosono, H. Iron-based layered superconductor La[O(1−x)F(x)]FeAs (x = 0.05–0.12) with T(c) = 26 K. *J. Am. Chem. Soc.* **2008**, *130*, 3296–3297. [CrossRef]
6. Mizuguchi, Y.; Demura, S.; Deguchi, K.; Takano, Y.; Fujihisa, H.; Gotoh, Y.; Izawa, H.; Miura, O. Superconductivity in novel BiS2-based layered superconductor $LaO_{1-x}F_xBiS_2$. *J. Phys. Soc. Jpn.* **2012**, *81*, 114725. [CrossRef]
7. Xing, J.; Li, S.; Ding, X.; Yang, H.; Wen, H.-H. Superconductivity appears in the vicinity of semiconducting-like behavior in $CeO_{1-x}F_xBiS_2$. *Phys. Rev. B* **2012**, *86*, 214518. [CrossRef]
8. Jha, R.; Kumar, A.; Singh, S.K.; Awana, V.P.S. Synthesis and Superconductivity of New BiS_2 Based Superconductor $PrO_{0.5}F_{0.5}BiS_2$. *J. Supercond. Nov. Magn.* **2013**, *26*, 499–502. [CrossRef]
9. Demura, S.; Mizuguchi, Y.; Deguchi, K.; Okazaki, H.; Hara, H.; Watanabe, T.; Denholme, S.J.; Fujioka, M.; Ozaki, T.; Fujihisa, H.; et al. New Member of BiS_2-Based Superconductor $NdO_{1-x}F_xBiS_2$. *J. Phys. Soc. Jpn.* **2013**, *82*, 033708. [CrossRef]
10. Yazici, D.; Huang, K.; White, B.D.; Chang, A.H.; Friedman, A.J.; Maple, M.B. Superconductivity of F-substituted *Ln*$OBiS_2$ (*Ln* = La, Ce, Pr, Nd, Yb) compounds. *Philos. Mag.* **2013**, *93*, 673. [CrossRef]
11. Kinami, K.; Hanada, Y.; Nagao, M.; Miura, A.; Goto, Y.; Maruyama, Y.; Watauchi, S.; Takano, Y.; Tanaka, I. Growth of Superconducting Sm(O,F)BiS_2 Single Crystals. *Cryst. Growth Des.* **2019**, *19*, 6136–6140. [CrossRef]
12. Nagao, M.; Miura, A.; Ueta, I.; Watauchi, S.; Tanaka, I. Superconductivity in $CeOBiS_2$ with cerium valence fluctuation. *Solid State Commun.* **2016**, *245*, 11–14. [CrossRef]
13. Tanaka, M.; Nagao, M.; Matsumoto, R.; Kataoka, N.; Ueta, I.; Tanaka, H.; Watauchi, S.; Tanaka, I.; Takano, Y. Superconductivity and its enhancement under high pressure in "F-free" single crystals of $CeOBiS_2$. *J. Alloys Compd.* **2017**, *722*, 467–473. [CrossRef]
14. Hanada, Y.; Nagao, M.; Miura, A.; Maruyama, Y.; Watauchi, S.; Takano, Y.; Tanaka, I. Growth and characterization of (La,Ce)$OBiS_2$ single crystals. *Jpn. J. Appl. Phys.* **2019**, *58*, 063001. [CrossRef]
15. Miura, A.; Nagao, M.; Goto, Y.; Mizuguchi, Y.; Matsuda, T.D.; Aoki, Y.; Moriyoshi, C.; Kuroiwa, Y.; Takano, Y.; Watauchi, S.; et al. Crystal Structure and Superconductivity of Tetragonal and Monoclinic $Ce_{1-x}Pr_xOBiS_2$. *Inorg. Chem.* **2018**, *57*, 5364–5370. [CrossRef]
16. Nagao, M.; Miura, A.; Urushihara, D.; Maruyama, Y.; Goto, Y.; Mizuguchi, Y.; Moriyoshi, C.; Kuroiwa, Y.; Wang, Y.; Watauchi, S.; et al. Flux Growth and Superconducting Properties of (Ce,Pr)$OBiS_2$ Single Crystals. *Front. Chem.* **2020**, *8*, 44. [CrossRef]
17. Kase, N.; Matsumoto, M.; Kondo, K.; Gouchi, J.; Uwatoko, Y.; Sakakibara, T.; Miyakawa, N. Superconductivity of Electron-Doped $NdOBiS_2$ by Substitution of Mixed-Valence Ce Ions. *J. Phys. Soc. Jpn.* **2019**, *88*, 103703. [CrossRef]
18. Fujita, Y.; Kinami, K.; Hanada, Y.; Nagao, M.; Miura, A.; Hirai, S.; Maruyama, Y.; Watauchi, S.; Takano, Y.; Tanaka, I. Growth and Characterization of $ROBiS_2$ High-Entropy Superconducting Single Crystals. *ACS Omega* **2020**, *5*, 16819–16825. [CrossRef]
19. Higashinaka, R.; Asano, T.; Nakashima, T.; Fushiya, K.; Mizuguchi, Y.; Miura, O.; Matsuda, T.D.; Aoki, Y. Pronounced −Log *T* Divergence in Specific Heat of Nonmetallic $CeOBiS_2$: A Mother Phase of BiS_2-Based Superconductor. *J. Phys. Soc. Jpn.* **2015**, *84*, 023702. [CrossRef]
20. Nagao, M.; Miura, A.; Matsumoto, R.; Maruyama, Y.; Watauchi, S.; Takano, Y.; Tadanaga, K.; Tanaka, I. Growth and transport properties under high pressure of $PrOBiS_2$ single crystals. *Solid State Commun.* **2019**, *296*, 17–20. [CrossRef]
21. Nagao, M.; Demura, S.; Deguchi, K.; Miura, A.; Watauchi, S.; Takei, T.; Takano, Y.; Kumada, N.; Tanaka, I. Structural Analysis and Superconducting Properties of F-Substituted $NdOBiS_2$ Single Crystals. *J. Phys. Soc. Jpn.* **2013**, *82*, 113701. [CrossRef]
22. Nagao, M. Growth and characterization of R(O,F)BiS_2 (R = La, Ce, Pr, Nd) superconducting single crystals. *Nov. Supercond. Mater.* **2015**, *1*, 64–74. [CrossRef]
23. Yaroslavtsev, A.; Menushenkov, A.; Chernikov, R.; Clementyev, E.; Lazukov, V.; Zubavichus, Y.; Veligzhanin, A.; Efremova, N.; Gribanov, A.; Kuchin, A. Ce valence in intermetallic compounds by means of XANES spectroscopy. *Z. Krist. Cryst. Mater.* **2010**, *225*, 482. [CrossRef]
24. Yamazaki, S.; Matsui, T.; Ohashi, T.; Arita, Y. Defect structures in doped CeO_2 studied by using XAFS spectrometry. *Solid State Ion.* **2000**, *136–137*, 913–920. [CrossRef]
25. Ku, H.C.; Lin, B.N.; Lin, Y.X.; Hsu, Y.Y. Effect of Pr–O hybridization on the anomalous magnetic properties of $Pr_{1+x}Ba_{2-x}Cu_3O_{7-y}$ system. *J. Appl. Phys.* **2002**, *91*, 7128. [CrossRef]
26. Lin, B.N.; Lin, Y.X.; Hsu, Y.Y.; Liao, J.D.; Cheng, W.H.; Lee, J.F.; Jang, L.Y.; Ku, H.C. Anomalous Pr Ordering, PrL_3-Edge and Cu *K*-Edge XANES Studies for the Insulating $PrBa_2Cu_3O_{7-y}$ System. *J. Low Temp. Phys.* **2003**, *131*, 803. [CrossRef]
27. Fujishiro, H.; Naito, T.; Ogawa, S.; Yoshida, N.; Nitta, K.; Hejtmánek, J.; Knížek, K.; Jirák, Z. Valence Shift of Pr Ion from 3+ to 4+ in $(Pr_{1-y}Y_y)_{0.7}Ca_{0.3}CoO_3$ Estimated by X-Ray Absorption Spectroscopy. *J. Phys. Soc. Jpn.* **2012**, *81*, 064709. [CrossRef]

28. Shannon, R.D. Revised effective ionic radii and systematic studies of interatomic distances in halides and chalcogenides. *Acta Crystallogr. Sect. A* **1976**, *32*, 751–767. [CrossRef]
29. Mizuguchi, Y.; Miura, A.; Kajitani, J.; Hiroi, T.; Miura, O.; Tadanaga, K.; Kumada, N.; Magome, E.; Moriyoshi, C.; Kuroiwa, Y. In-plane chemical pressure essential for superconductivity in $BiCh_2$-based (Ch: S, Se) layered structure. *Sci. Rep.* **2015**, *5*, 14968. [CrossRef]